Case studies of aerosol remote sensing in the vicinity of clouds

Jens Redemann,[1] Qin Zhang,[1] Philip B. Russell,[2] John M. Livingston,[3] and Lorraine A. Remer[4]

Received 14 July 2008; revised 28 August 2008; accepted 12 December 2008; published 26 March 2009.

[1] Studying the spatial variability of aerosol properties in the vicinity of clouds is essential to our ability to determine aerosol direct and indirect effects on climate. In this paper, we describe aerosol observations collected near cloud edges by an airborne Sun photometer over dark ocean waters. Focusing on case studies of aerosol measurements near eight cloud edges within a dissipating stratiform cloud deck, we compare the airborne Sun photometer observations to retrievals of aerosol properties using the standard Moderate Resolution Imaging Spectroradiometer (MODIS) aerosol algorithm applied to 500-m-resolution MODIS spectral reflectances. We find a persistent, spectrally neutral increase in the Sun photometer–derived aerosol optical depth (AOD) of up to 10% (0.015) in the 2-km distances closest to the edges of several distinct clouds. At midvisible wavelengths, the MODIS AOD retrievals show similar increases toward cloud edges, although a larger increase in AOD is found in the MODIS along-scan direction. At shortwave infrared (SWIR) wavelengths (1240–2130 nm), the MODIS-derived AOD increases near cloud edges are of the order of 0.03 and as such three times as large as the Sun photometer–derived values. Hence, in contrast to recently discussed "bluing" of aerosols near cloud edges, i.e., a preferential apparent increase in the visible reflectances of clear-sky pixels due to 3-D radiative transfer effects in the vicinity of clouds, we find a "reddening" of aerosols in the MODIS 500-m-resolution aerosol retrievals near clouds. This "reddening" in our study can be traced to larger absolute increases in SWIR reflectances when compared to visible reflectances near clouds, which in turn seem to stem from larger electronic cross talk in the MODIS SWIR bands (5–7). We note that the lack of "bluing" in our MODIS observations is likely due to the small geometric and optical thicknesses of the clouds considered.

Citation: Redemann, J., Q. Zhang, P. B. Russell, J. M. Livingston, and L. A. Remer (2009), Case studies of aerosol remote sensing in the vicinity of clouds, *J. Geophys. Res.*, *114*, D06209, doi:10.1029/2008JD010774.

1. Introduction

[2] Our ability to assess aerosol effects on climate using remote-sensing data depends on the discrimination between cloudy and cloud-free viewing elements. In the case of the direct aerosol radiative forcing of climate it is essential to avoid subpixel cloud contamination of pixels used for aerosol clear-sky retrievals, while including areas of potentially increased aerosol concentration or size in the vicinity of clouds, often referred to as "cloud halos" [e.g., *Radke and Hobbs*, 1991; *Perry and Hobbs*, 1996; *Flossmann*, 1998; *Koren et al.*, 2007]. In the case of the indirect and semidirect aerosol effects on climate it is also mandatory to distinguish cloudy from cloud-free pixels, while ensuring spatial proximity of the aerosol and cloud air masses that are supposedly linked through indirect effects. Therefore, studying aerosol properties as well as their spatial variability in the vicinity of clouds is essential to our ability to separate aerosol and cloudy pixels in remotely sensed data, to our ability to interpret remotely sensed data in between cloudy pixels, and hence to determine aerosol effects on climate at different spatial scales.

[3] The current generation of satellite aerosol sensors, such as the Moderate Resolution Imaging Spectroradiometer (MODIS) [*Kaufman et al.*, 1997] and the Multiangle Imaging Spectroradiometer (MISR) [*Kahn et al.*, 2001] aboard the Terra satellite, MODIS aboard Aqua, and the Ozone Monitoring Instrument (OMI) aboard Aura [*Levelt et al.*, 2006] are much more capable of detailed global aerosol observations than the previous generation, including the Total Ozone Mapping Spectrometer (TOMS) and the Advanced Very High Resolution Radiometer (AVHRR). The advantages of the new sensors include their improved spectral coverage, narrower bandwidth of the individual channels and improved spatial resolution. Spatial variability in radiance fields observed by passive satellite sensors is frequently used in the separation of cloud and aerosol signals, under the assumption that most clouds exhibit larger spatial variability than aerosols do [*Martins et al.*, 2002]. However, a variability-based

[1]BAER Institute, Sonoma, California, USA.
[2]NASA Ames Research Center, Moffett Field, California, USA.
[3]SRI International, Menlo Park, California, USA.
[4]NASA Goddard Space Flight Center, Greenbelt, Maryland, USA.

Copyright 2009 by the American Geophysical Union.
0148-0227/09/2008JD010774

cloud screening technique is likely to miss some of the aforementioned "cloud halos," in which the variability in aerosol properties may lead to variability in the satellite-observed reflectances. *Kaufman et al.* [2006, paragraph 1] pointed out that aerosol and cloud fields are often spatially correlated and that therefore, "rigorous cloud screening can systematically bias toward less cloudy and drier conditions, underestimating the average aerosol optical thickness (AOT)." Several studies [e.g., *Kaufman et al.*, 2005; *Redemann et al.*, 2006], found that differences between MODIS and suborbital AOD measurements were correlated with MODIS-derived cloud fraction, indicating the need for a renewed focus on cloud screening. However, only a small number of studies have been directed at assessing the variability of aerosol optical properties in the vicinity of clouds [e.g., *Redemann et al.*, 2006; *Koren et al.*, 2007] because only a small number of suitable instruments exists.

[4] Besides the issue of subpixel cloud contamination, there are 3-D radiative transfer considerations that are relevant for passive satellite remote sensing of aerosols in the vicinity of clouds [*Nikolaeva et al.*, 2005; *Zhang et al.*, 2005; *Wen et al.*, 2006; *Yang and Di Girolamo*, 2008; *Kassianov and Ovtchinnikov*, 2008; *Marshak et al.*, 2008]. In support of findings by *Kaufman et al.* [2005] that aerosol fine mode fraction increases in the vicinity of clouds, *Marshak et al.* [2008] presented a conceptual model that leads to a "bluing" of aerosols, i.e., a preferential apparent increase in the visible reflectances of clear-sky pixels due to 3-D radiative transfer effects near clouds. This "bluing" is essentially a result of the fact that the increased reflectance of the cloud-adjacent clear column is largely modulated by molecular scattering. For example, *Wen et al.* [2006] found that 3-D radiative transfer effects in a broken cumulus cloud field embedded in background biomass burning aerosol with an AOD of 0.1 could reach as far as 3 km away from clouds and cause an overestimate of the apparent clear sky reflectance that would lead to an overestimate in AOD by 40%. As *Marshak et al.* [2008] point out, these results depend heavily on factors such as cloud geometry, aerosol layer location, and surface reflectance. These 3-D radiative transfer effects have the diametrically opposite effect of subpixel cloud contamination, which would tend to increase the aerosol coarse mode fraction near clouds.

[5] The purpose of this paper is to describe our recent efforts in studying the aerosol-cloud boundary using simultaneous airborne Sun photometer and MODIS reflectance measurements. We describe aerosol observations collected near cloud edges by the NASA Ames Airborne Tracking Sunphotometer (AATS-14) deployed on the CIRPAS Twin-Otter research aircraft in EVE (Extended-MODIS-λ Validation Experiment) [*Redemann et al.*, 2006] off the Northern California coast in April 2004. The primary purpose of EVE was the validation of MODIS retrievals of spectral AOD from the visible to the near IR using measurements taken by AATS-14. In the period from 16 to 30 April 2004, the CIRPAS Twin-Otter aircraft flew seven research flights, each focused on measurements outside of MODIS glint, but inside an area with satellite elevation angles greater than 30 degrees. During these flights, AATS-14 captured four MODIS-Terra (16, 21, 26 and 28 April) and four MODIS-Aqua (21, 26, 28 and 30 April) overpasses. On most days in EVE, we attempted to make measurements in the presence of Asian mineral dust transported across the Pacific to maximize AOD at the SWIR wavelengths. As is typical for the California coast in Spring, most days had some presence of low-level stratus decks. The case we focused on in this paper took place on 30 April 2006. We focused on this case study because the airborne Sun photometer measurements indicated an increase in AOD near cloud edges without a concurrent change in the Angstrom exponent. As pointed out in section 2.1.2, this is the only scenario in which we can be highly confident that the airborne Sun photometer measurements are not themselves contaminated by clouds. Indeed, we have many observations that show AOD changes near clouds that are concurrent with changes in the Angstrom exponent. The analysis of these cases will be left to a future paper as such analyses would require a more detailed look at the issue of possible cloud contamination in the Sun photometer measurements.

[6] To facilitate the comparisons of the high spatial resolution airborne observations to the MODIS observations near clouds in this paper, we applied the standard MODIS aerosol retrieval algorithm [*Remer et al.*, 2005] to spectral MODIS reflectances at 500-m resolution. This process yielded aerosol retrievals at 500×500 m^2 resolution (hereafter referred to as 500-m-resolution), which in turn allowed the study of aerosol optical depth as a function of distance from cloud edges. The airborne Sun photometer observations have the advantages of (1) being full column so as to allow direct comparison to satellite AOD measurements, (2) being over dark ocean waters, and (3) being much less affected by 3-D radiative transfer effects such as those that cause apparent reflectance increases near clouds in satellite observations, and if affected then in the direction toward decreased AOD (see section 2.1 for a more detailed explanation).

2. Aerosol Observations Near Clouds

2.1. NASA Ames Airborne Tracking Sunphotometer, AATS-14

2.1.1. General Description of Airborne Sun Photometer Data

[7] AATS-14 measures direct solar beam transmission in 14 narrow channels (with bandwidths between 2 and 5.6 nm for the wavelengths between 354 and 1558 nm and 17.3 nm for the 2139-nm channel) by using detectors in a tracking head that is mounted externally to the aircraft. From the measured slant-path transmissions we derive spectral AOD in 13 wavelength bands at (354, 380, 453, 499, 519, 604, 675, 778, 864, 1019, 1240, 1558 and 2139 nm) [*Russell et al.*, 1999; *Redemann et al.*, 2006]. The two channels at 1558 and 2139 nm are temperature-controlled at 0°C; all other channels are temperature-controlled at 45°C. In addition to the corrections for Rayleigh scattering and O_3 absorption, some channels require corrections for NO_2, H_2O and O_2-O_2 absorption. Cross sections were computed using LBLRTM 6.01 [*Clough and Iacono*, 1995] with the CKD 2.4.1 continuum model using the HITRAN 2000 (v 11.0) line list [*Rothman et al.*, 2001; *Rothman and Schroeder*, 2002] (including an update for water vapor from April 2001; see http://www.hitran.com/hitran/updates.html). NO_2 cross sections not included in LBLRTM 6.01 were taken from *Harder et al.* [1997]. NO_2 was assumed constant

at 2×10^{-15} molecules cm^{-2}. Column ozone estimates are taken from TOMS satellite observations. The AATS-14 instrument and data recording are described by *Schmid et al.* [2000] and *Russell et al.* [2005]. Our methods for further data reduction, calibration, and error analysis are described by *Russell et al.* [1993], *Schmid and Wehrli* [1995], and *Schmid et al.* [2001]. Radiometric calibration of AATS-14 is determined using the Langley plot technique [*Schmid and Wehrli*, 1995]. For EVE, AATS-14 was calibrated at the Mauna Loa Observatory, Hawaii, in March and June of 2004, bracketing the EVE campaign. Owing to filter degradation, the calibration constants obtained from the postmission calibration were generally lower than the premission calibration. However, for eleven of the thirteen aerosol channels the change was 0.5% or less. The two remaining channels (380 and 1240 nm) had degraded by about 1%. We assumed a linear temporal variation between the premission and postmission calibration constants, considering their change by including a statistical uncertainty equal to half the range between premission and postmission calibration. Relevant for this study is that after consideration of all possible sources of error, the AATS-14 derived AOD had the highest uncertainties for those channels with the largest difference in premission and postmission calibration. For the seven AATS-14 wavelengths closest to the MODIS AOD retrieval wavelengths (i.e., AATS wavelengths of 453, 519, 675, 864, 1240, 1558 and 2139 nm), the mean uncertainties in AOD between 2136 UT and 2145 UT on 30 March 2004, at a mean aerosol air mass factor of 1.15, were 0.004, 0.004, 0.003, 0.002, 0.005, 0.002, and 0.003, respectively. Note that the largest uncertainty was calculated for the 1240-nm channel, which was the channel with the largest difference between premission and postmission calibration as mentioned above. AATS-14 data collected in EVE is available at http://geo.arc.nasa.gov/sgg/EVE-website/data/data.html.

2.1.2. Cloud Screening of Airborne Sun Photometer Data

[8] Cloud screening of the AATS-14 derived AOD relies mostly on the spatial variability of the transmission measurements. AATS-14 records direct solar beam transmissions every four seconds. Within the first three of the 4-s intervals nine distinct measurements are taken, the standard deviation of which is compared to a threshold level to determine possible cloud contamination. Similar to the basic cloud screening of MODIS reflectances described in the following section, this method assumes that an aerosol field is spatially more homogeneous than a cloud field. As long as the AATS instrument maintains tracking of the solar disk through or near a cloud, the Angstrom exponent of aerosol retrievals is a second test of the effectiveness of the cloud screening method in the following manner: if a 3-s data sample is indicated as being cloud contaminated by the variability method, yet the Angstrom exponent is the same as that calculated from adjacent observations that were spatially homogeneous, we assume that the method is too aggressive and that the cloud detection threshold can be relaxed, until only data points with Angstrom exponents lower than the background aerosol are being screened. If, however, a 3-s data sample is indicated as being cloud contaminated by the variability method and the Angstrom exponent of an aerosol retrieval based on that sample is lower than the Angstrom exponent of previous data points, we have to assume that our method works correctly, i.e., a cloud section has entered the instrument field of view, and the cloud threshold cannot be relaxed further. We note that this method is prone to flag areas of increased aerosol particle size in the vicinity of clouds as cloudy, if the change in particle properties results in a significant variability of the transmission measurements. However, the opposite is not true: if an AOD gradient without an Angstrom exponent change is present in the vicinity of a cloud, our method will correctly identify such a region as aerosol. We note further that 3-D scattered photons out of the side of adjacent clouds, such as those that increase the apparent clear-sky reflectance in satellite observations [e.g., *Marshak et al.*, 2008], would tend to cause an increase in the AATS-measured transmission, resulting in a decreased AOD retrieval. Therefore, we are confident that increases of aerosol optical depth near clouds without associated Angstrom exponent changes are correctly identified in the airborne Sun photometer measurements. Finally, we note that an AATS data recording every four seconds results in a spatial resolution of about 200 m, assuming an aircraft speed of 100 knots, which was typical for the CIRPAS Twin-Otter in EVE.

2.2. MODIS Aerosol Observations

[9] The standard MODIS over-ocean algorithm for the retrieval of aerosol optical depth aggregates the reflectances from the six channels at 553, 644, 855, 1243, 1632 and 2119 nm into nominal 10-km boxes of 20 by 20 pixels at 500-m resolution [*Remer et al.*, 2005]. The algorithm uses the difference in spatial variability between aerosols and clouds for the identification of clouds [*Martins et al.*, 2002]. Specifically, the standard deviation of 553-nm reflectances of a square set of 3×3 500-m pixels are compared to a threshold value of 0.0025. If the standard deviation is larger than the threshold value the center pixel is declared "cloudy" and the set of 3×3 pixels is moved in such a way that a pixel neighboring the previous center pixel is now the center pixel. The result is a cloud mask at an effective resolution of 500 m. Details of the aerosol retrieval algorithm can be found in *Remer et al.*, 2005. For the purpose of this paper, i.e., the study of aerosol properties within a few kilometers of clouds, the 10×10 km^2 resolution standard MODIS aerosol product is too coarse. We therefore, adopted the algorithm for our purpose, by applying it to the MODIS reflectance spectra at the native resolution of 500 m for those pixels which passed the spatial variability test. The required input parameters for describing the exact viewing geometry for each pixel were taken from the native MODIS L1B data files. It should be noted that the pixel-selection procedure used here is different from the procedure used in the production of the standard MODIS aerosol product (MOD04_L2/MYD04_L2) in that the standard procedure also eliminates the 25% darkest and brightest pixels (in terms of reflectances at 553 nm) from further analysis. We justify our choice to not eliminate those pixels because our primary objective here is to study the information content of MODIS reflectance measurements near clouds, rather than a test of the possible limitations of the MOD04_L2 product.

3. Results

[10] The airborne Sun photometer observations on 30 April 2004 are shown in Figure 1. On this day the flight

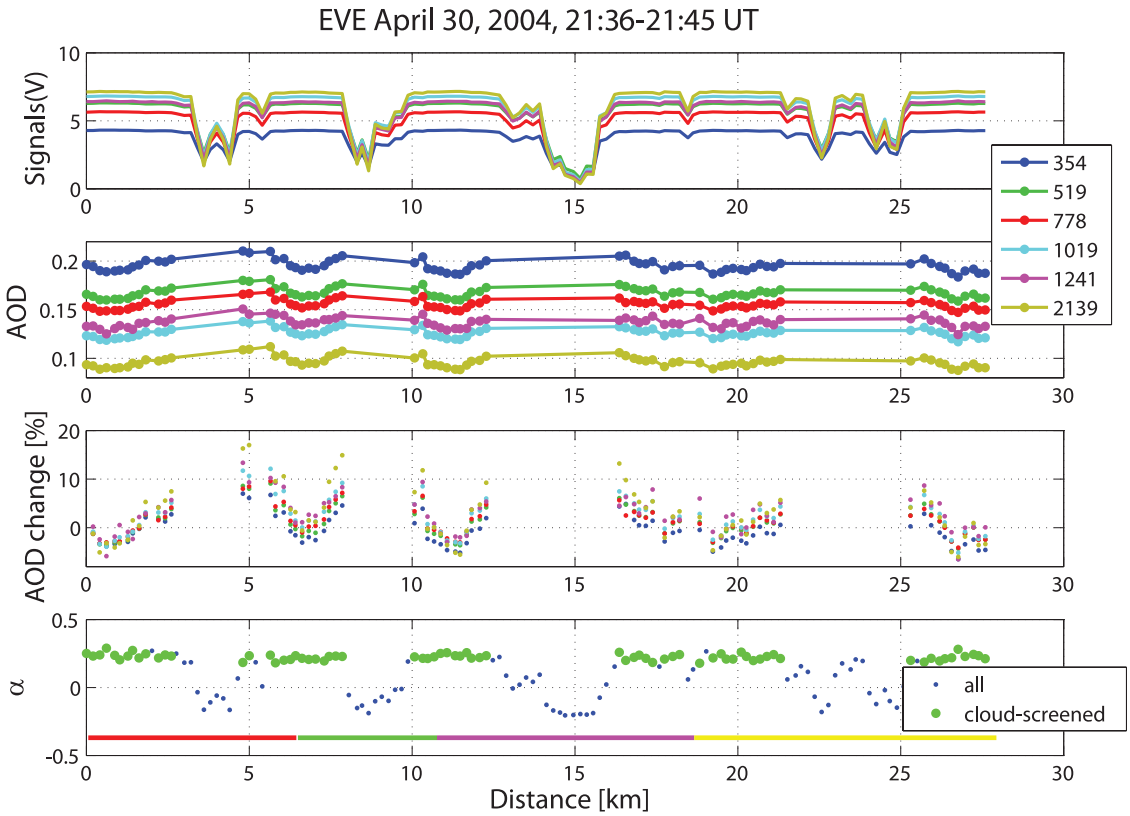

Figure 1. Traces of AATS signal voltages, derived AOD, relative AOD, and modified Angstrom exponent (see text). Colored, straight lines in the fourth plot denote the location of the flight track segments indicated in Figure 2.

path was near the edge of a dissipating stratus cloud deck over dark water off the Coast of Monterey, California. The MODIS cloud observations for this day (not shown) indicated cloud top heights below 2000 m and there were a few sparse retrievals of cloud optical depth below 2. The airborne Sun photometer maintained tracking of the Sun even through clouds, allowing for a continuous time series of transmission and hence AOD measurements. The top set of plots in Figure 1 shows the signal voltage in the six AATS channels at 354, 519, 778, 1019, 1241 and 2139 nm, measured during a low-level flight leg at an average altitude of 32 m above sea level with only small variations in altitude of ±10 m. These data are plotted versus the distance traveled from an arbitrarily chosen point along the flight track. There are four troughs in the signal traces, indicating four distinct clouds, between which AATS was taking clear sky measurements. The second set of plots in Figure 1 shows the cloud-screened AOD traces calculated from the signals in the top set of plots. Note the lack of AOD retrievals at those locations where the signal variability indicated cloud contamination. In the third set of plots, we show the relative change of spectral AOD to the AOD at the starting point of this flight segment. We chose this plotting style to emphasize the troughs in AOD observations in between clouds, i.e., the relatively larger AOD near cloud edges and the return to background AOD levels in between clouds. Finally, the fourth set of plots indicates the so-called modified Angstrom exponent, i.e., the coefficient of the linear term in a quadratic fit of the logarithm of AOD versus the logarithm of wavelength (using the 13 AATS aerosol wavelengths listed at the start of section 2.1.1). Green data points indicate Angstrom exponents of AOD spectra that have passed the spatial variability test, while blue data points indicate measurements that were spatially too variable and hence are flagged as cloud-contaminated. Note how most of the blue data points show smaller Angstrom exponents, which are usually associated with cloud retrievals. As pointed out in section 2.1, this is an independent test of the effectiveness of the AATS cloud screening.

[11] As pointed out in section 2, the AATS observations shown in Figure 1 are at much finer spatial resolution, generally 200 m or finer, than the standard MODIS aerosol retrievals in MOD04_L2, which is usually reported at a resolution of 10 × 10 km (at nadir). Therefore, we modified the standard algorithm that produces MOD04_L2 and applied it to MODIS-Aqua reflectance spectra at the native resolution of 500 × 500 m^2, after calculating the required input parameters describing the viewing geometry for each pixel.

[12] Figure 2a shows a map of midvisible 500-m-resolution MODIS retrievals of AOD at 550 nm thus obtained from the MODIS-Aqua overpass at 2130 UT. The mean solar zenith angle for all 1,200 pixels was 29.0° and the mean solar azimuth angle was 226.5° (measured clockwise from N). White edges around individual 500-m pixels denote where the MODIS spatial variability mask indicates a cloud. These pixels would not be used to compute an average 10 × 10 km^2

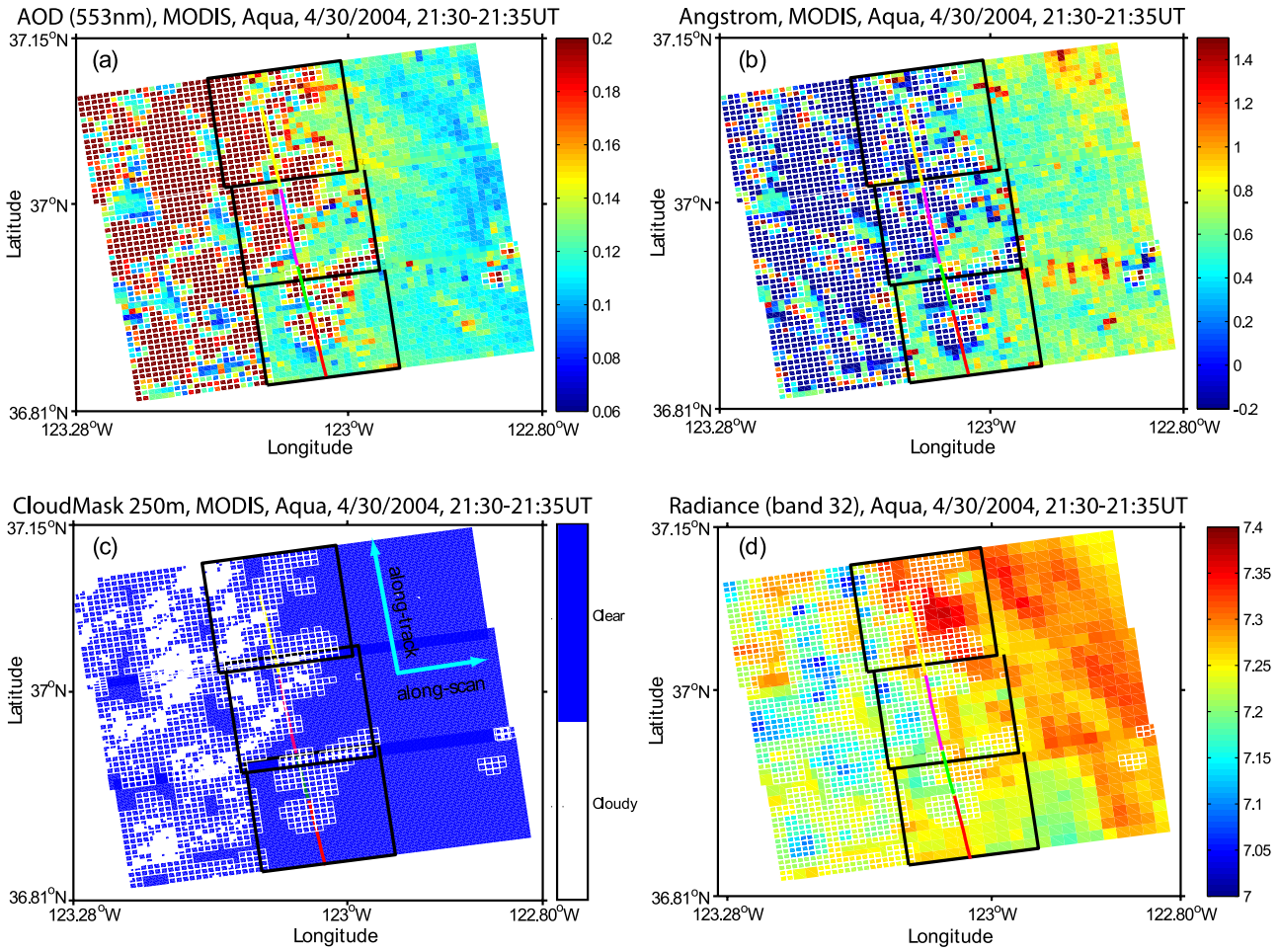

Figure 2. (a) Map of 500 × 500 m resolution MODIS-like 553-nm AOD retrievals. MODIS pixels that are considered cloudy by the spatial variability test of adjacent reflectances are indicated by white borders. Pixels without white borders are considered cloud-free, and their AOD is given by the color bar on the right. Note that pixels with white borders are considered cloudy; the optical depth retrievals in these boxes are likely incorrect because of the application of an aerosol retrieval algorithm. This fact is irrelevant for our analysis, as we do not use the retrievals in the cloudy pixels any further. The aircraft flight track during which the data in Figure 1 were acquired is also shown, with different colors indicating flight segments in the vicinity of individual clouds. The large black boxes represent the 10 × 10 km areas for which the standard MODIS aerosol product MOD04_L2 is available. (b) Retrieval map of the Angstrom exponent calculated from AOD at 553 nm and 865 nm. (c) Retrieval map of the MODIS standard cloud mask MOD35 at a resolution of 250 m. (d) Map of MODIS band 32 (11 μm) radiances.

reflectance for subsequent retrieval of aerosol properties by the standard MODIS aerosol product. Also shown in Figure 2 is the aircraft flight track during which the data in Figure 1 were acquired, with different colors indicating flight segments in the vicinity of individual clouds. A study of Figure 2a reveals quickly that most of the MODIS pixels along the aircraft flight track are cloud-screened. There are a number of reasons for the fact that the airborne Sun photometer observations are indicated as cloud-free while the collocated MODIS observations show cloud contamination. First, the MODIS reflectance measurements are taken nearly instantaneously, while the aircraft observations take a finite amount of time, in this case about nine minutes to acquire. Therefore, it is possible that clouds that were present in a given MODIS pixel moved away and are no longer present at the time the aircraft passes the same pixel. Second, as mentioned above, the variability in aerosol properties observed in the aircraft measurements caused sufficient variability in the satellite reflectances for the pixels along the aircraft track to fail the spatial variability based cloud screening. Third, it is possible that these pixels are contaminated by small-scale clouds that still allow in-between cloud AOD measurements with AATS-14.

[13] To overcome the lack of exactly collocated MODIS and AATS observations that are indicated as cloud-free within the context of the cloud screening of each instrument, we compare the aircraft observations to the MODIS retrievals in a statistical sense. In Figure 3a, we therefore plot all AATS retrievals of AOD at 519 nm as a function of distance away from the nearest cloud edge for all clouds identified in the aircraft measurements (see Figure 1). Along the aircraft flight track indicated in Figure 2, there were a

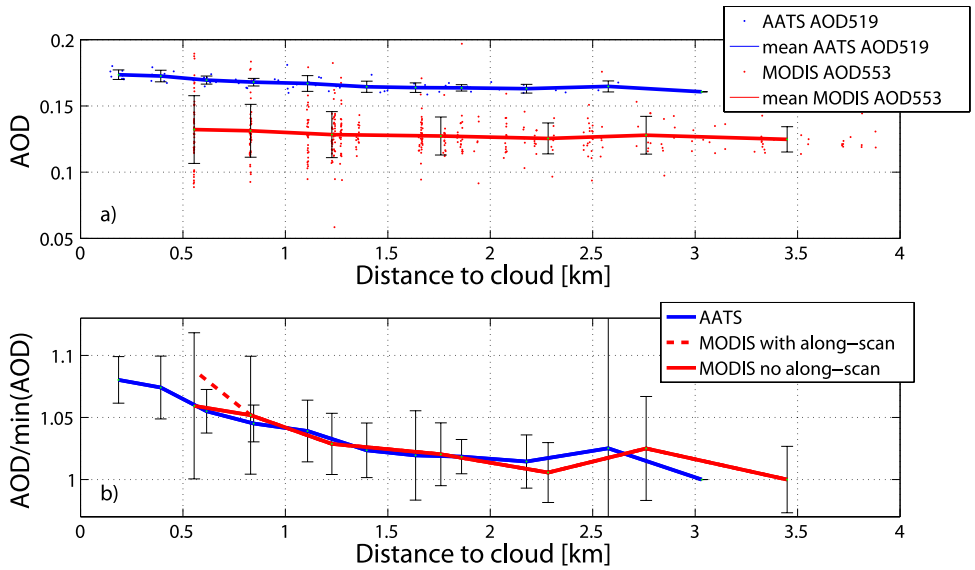

Figure 3. (a) MODIS (red) and AATS-derived (blue) midvisible AOD as a function of distance from nearest cloud edge. Solid lines connect the mean of MODIS and AATS derived AOD, binned in such a way as to create roughly equal numbers of individual observations in each distance interval. (MODIS distances are between pixel centers; this can yield a distance of $\sqrt{2} \times 500$ m for diagonally adjacent pixels at nadir, etc.) (b) Relative change in AOD as determined by both instruments. The dashed, red line shows the MODIS observations when all cloud-adjacent pixels in the MODIS along-scan direction are considered. The solid line shows the MODIS reflectances when 500-m pixels adjacent to clouds in MODIS along-scan direction are omitted. Unlike the error bars in Figure 3a, which represent the standard deviation of all observations in a given distance interval, the error bars in Figure 3b represent 95% confidence intervals of a *T* test of the null hypothesis that the increase in AOD in a given distance relative to the minimum AOD value at the farthest distance from cloud is significant (at the 95% confidence level; see text). Note that the MODIS uncertainties limits do not extend down to 1 for distances less than 1.5 km, indicating that the AOD increases at those distances are significant beyond 95% confidence.

total of 69 spectral AOD observations by AATS. We then binned the AATS AOD observations in such a way as to create distance bins with roughly equal numbers of AATS data points, resulting in bin width between 250 and 500 m. The blue line in Figure 3a represents the average AATS AOD in each distance interval, with the error bars representing the standard deviation of all AATS AOD retrievals in each bin. We applied the same procedure to all MODIS 500-m-resolution AOD retrievals inside the three 10×10 km^2 black boxes indicated in Figure 2. Out of a total of 1,200 500-m-resolution MODIS spectral reflectance measurements in the three black boxes, 461 reflectance spectra passed the spatial variability test (average cloud fraction: $(1200-461)/1200 \approx 62\%$) and were used to retrieve spectral AOD. These 461 MODIS AOD observations were then binned into distance intervals of approximately equal number, and their average and standard deviation are plotted as red lines in Figure 3 as a function of distance from the closest cloud edge as identified by the MODIS spatial variability test (i.e., white boxes in Figure 2). We did not perform a wavelength interpolation in the AATS data because (1) the AATS observations indicated very small Angstrom exponents, i.e., spectral change in AOD, and (2) we are mostly interested in relative changes in AOD as a function of distance away from cloud edges. Figure 3b then shows the relative change in AATS- and MODIS-derived midvisible AOD as a function of distance away from the nearest cloud edge. The solid, red line shows the MODIS observations when all cloud-adjacent pixels in the MODIS along-scan direction are considered. The dashed line shows the MODIS observations when 500-m pixels adjacent to clouds in MODIS along-scan direction are omitted. Note that the latter method results in somewhat better agreement with the Sun photometer observations, suggesting that there is a cloud adjacency effect in the MODIS reflectance observations that is more pronounced in the MODIS along-scan direction. These results are in general agreement with findings by *Meister et al.* [2008], which showed that the contamination of clear pixels near bright targets in MODIS-Aqua band 16 was asymmetric, with more pixels requiring screening in the along-scan direction. Unlike the error bars in Figure 3a, which represent the standard deviation of all observations in a given distance interval, the error bars in Figure 3b represent 95% confidence intervals of a *T* test [e.g., *Spiegel et al.*, 2000] of the null hypothesis that the increase in AOD toward cloud edge relative to the minimum AOD value at the farthest distance from cloud is significant (at the 95% confidence level). Note that the MODIS uncertainty limits do not extend down to 1 for distances less than 1.5 km, indicating that the AOD increases at those distances are significant beyond 95% confidence. At distances greater than 1.5 km, both the AATS and MODIS AOD show confidence intervals that often extend below 1, indicating that at those distances the AOD increases are not statistically significant.

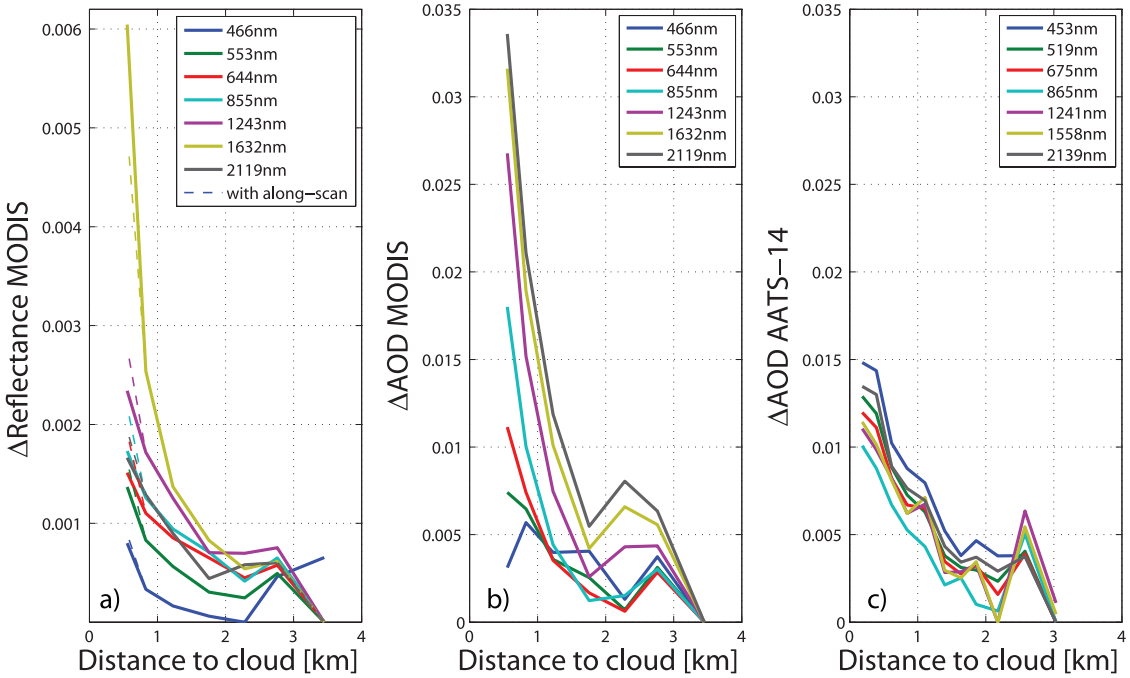

Figure 4. (a) Absolute change in MODIS reflectance from minimum value obtained in the 4 km closest to a cloud edge for all MODIS bands considered in the standard aerosol retrieval algorithm and all cloud-free 500-m pixels shown in Figure 2. As in Figure 3, the solid lines show the MODIS observations when 500-m pixels adjacent to clouds in MODIS along-scan direction are omitted. (b) Same as Figure 4a, but for the spectral AOD derived from MODIS. (c) Airborne Sun photometer–derived change in spectral AOD as a function of distance from cloud edge.

[14] To investigate the spectral dependence of the MODIS and AATS derived AOD increases near clouds, Figure 4a shows the absolute difference in reflectance of all seven MODIS bands employed in the standard aerosol retrieval algorithm (bands 1–7) as a function of distance from the nearest cloud edge (again as defined by the 3 × 3-std variability method, in complete correspondence to the one-wavelength observations shown in Figure 3) relative to the minimum reflectance in each band observed over the 4-km distance. In analogy to Figure 3, Figures 4a and 4b show the mean of 461 MODIS 500-m-resolution reflectance measurements and AOD retrievals near clouds, respectively. Figure 4b shows the absolute difference in MODIS spectral AOD for all seven MODIS wavelengths, while Figure 4c shows the AATS observations for the channels spectrally closest to the MODIS bands. Figure 4a indicates that the largest absolute changes in MODIS reflectances near clouds occur for the SWIR bands (5–7, 1243–2119 nm). Logically, the largest changes in AOD near cloud edges are hence found at the same wavelengths. However, Figure 4c indicates that the increase in aerosol optical depth as indicated by AATS-14 was in essence spectrally neutral, with all increases of the order of 0.01 to 0015. A comparison of Figures 4b and 4c suggests that a retrieval of spectral aerosol optical depth near cloud edges based on MODIS 500-m reflectance spectra indicates a larger increase in the SWIR AOD, i.e., an increase in particle size and hence a "reddening" of aerosols near the clouds in our specific case study. This reddening is not found in the independent airborne Sun photometer observations, which yield a spectrally neutral increase in AOD near these clouds.

4. Conclusions

[15] In a study of airborne Sun photometer–derived AOD data near cloud edges collected in the EVE (Extended-MODIS-λ Validation Experiment) experiment off the Northern California coast in 2004, we found that in 75% of the cases there was an increase of up to 20% in AOD in the closest 2 km near the clouds. For the case studies in the vicinity of a dissipating stratiform cloud deck on 30 April 2004 considered in detail here, the near-cloud AOD increases occurred without increases in particle size as inferred from Sun photometer AOD wavelength dependence. We compared the airborne Sun photometer observations to retrievals of aerosol properties using the standard MODIS aerosol algorithm applied to 500-m-resolution MODIS-Aqua Collection 5 spectral reflectances. We found a persistent, spectrally neutral increase in the Sun photometer–derived AOD of up to 10% in the 2-km range closest to the edges of several distinct clouds. Our Sun photometer observations are consistent with an increased concentration of aerosols of the same size as the background aerosols. At midvisible wavelengths, the MODIS AOD retrievals showed increases similar to the Sun photometer–derived increases toward cloud edges, although a larger increase in AOD was found in the MODIS along-scan direction. At short-wave infrared wavelengths (1240–2119 nm), the MODIS derived AOD increases near cloud edges were considerably larger than the AATS derived values and are directly traceable to the larger

absolute increases in the SWIR reflectances when compared to the visible reflectances. We presented four independent pieces of evidence that residual cloud contamination is not a likely reason for our findings. First, there is a strong spectral dependence in the reflectance increases we observe, with the SWIR increases a factor of 3 larger than the increases in the visible. Cloud contamination should have resulted in a spectrally neutral increase in reflectances. Second, the standard MODIS cloud mask MOD35 at a resolution of 250 m shown in Figure 2c indicates no residual cloud contamination and instead suggests that the cloud screening method used in the standard MODIS aerosol algorithm and also used here is a more aggressive cloud screening method. Third, as suggested by one of the reviewers, we used a lower threshold of 0.0020 instead of 0.0025 in the screening of the spatial variability of 3×3 500-m pixels. The resulting reflectance increases near clouds were slightly lower, but showed qualitatively the same result, namely, larger increases in SWIR reflectances than in the visible. Finally, an investigation of MODIS band 32 radiances, also shown in Figure 2d, showed no clear decreases where the visible and SWIR reflectances showed increases, although the radiance decreases would have been expected if cloud contamination were a serious issue.

[16] Hence, in contrast to recently discussed "bluing" of aerosols near cloud edges due to 3-D radiative transfer effects [*Marshak et al.*, 2008], we found a "reddening" of aerosols in the MODIS 500-m-resolution AOD aerosol retrievals near clouds. This "reddening" was due to the larger absolute increases in SWIR reflectances near clouds, which in turn seem to stem from larger electronic cross talk in the MODIS SWIR bands (5–7). By electronic cross talk, we mean the effect by which the readout of clear pixels on the MODIS detector array is affected by adjacent, brighter pixels which in the case of a broken cloud field may be cloud-contaminated. This effect is usually described by the pixel Point Spread Function (PSF), which in the case of MODIS-Aqua is poorly characterized [*Meister et al.*, 2008].

[17] We note that the reddening we observe would be physically plausible, i.e., it could be explained by the mechanism of aerosol swelling due to the increased humidity near clouds, but that in the case study considered here, its most plausible explanation turns out to be a MODIS instrument artifact. This instrument artifact is likely to extend only a few pixels away from cloud edges, with less extent in the across-track direction than in the along-track direction. We further note that the lack of "bluing" in MODIS observations is likely due to the small geometric and optical thicknesses of the clouds considered. A more detailed analysis of the global reproducibility of our results is warranted because they have strong implications for aerosol-cloud interaction studies using MODIS observations. We conclude that airborne remote sensing of the aerosol-cloud boundary is a unique tool that could be supplemented by aerosol in situ measurements at cloud level to increase its usefulness for testing satellite retrievals of aerosols near clouds.

[18] **Acknowledgments.** The authors would like to thank Shana Mattoo (SSAI) for help with the adaptation and implementation of the MODIS standard aerosol retrieval algorithm. We are grateful to Larry Di Girolamo (University of Illinois) and two anonymous reviewers for useful comments on our manuscript. Funding through NASA grant EOS/03-0584-0647 is gratefully acknowledged.

References

Clough, S. A., and M. J. Iacono (1995), Line-by-line calculations of atmospheric fluxes and cooling rates: 2. Application to carbon dioxide, ozone, methane, nitrous oxide, and the halocarbons, *J. Geophys. Res.*, *100*, 16,519–16,535, doi:10.1029/95JD01386.

Flossmann, A. I. (1998), Interaction of aerosol particles and clouds, *J. Atmos. Sci.*, *55*(5), 879–887, doi:10.1175/1520-0469(1998)055<0879:IOAPAC>2.0.CO;2.

Harder, J. W., J. W. Brault, P. V. Johnston, and G. H. Mount (1997), Temperature dependent NO_2 cross sections at high spectral resolution, *J. Geophys. Res.*, *102*, 3861–3879, doi:10.1029/96JD03086.

Kahn, R., P. Banerjee, and D. McDonald (2001), The sensitivity of multiangle imaging to natural mixtures of aerosols over ocean, *J. Geophys. Res.*, *106*, 18,219–18,238, doi:10.1029/2000JD900497.

Kassianov, E. I., and M. Ovtchinnikov (2008), On reflectance ratios and aerosol optical depth retrieval in the presence of cumulus clouds, *Geophys. Res. Lett.*, *35*, L06807, doi:10.1029/2008GL033231.

Kaufman, Y. J., D. Tanré, L. A. Remer, E. Vermote, A. Chu, and B. N. Holben (1997), Operational remote sensing of tropospheric aerosol over land from EOS moderate resolution imaging spectroradiometer, *J. Geophys. Res.*, *102*, 17,051–17,067, doi:10.1029/96JD03988.

Kaufman, Y. J., I. Koren, L. A. Remer, D. Rosenfeld, and Y. Rudich (2005), The effect of smoke, dust and pollution aerosol on shallow cloud development over the Atlantic ocean, *Proc. Natl. Acad. Sci. U. S. A.*, *102*, 11,207–11,212, doi:10.1073/pnas.0505191102.

Kaufman, Y. J., G. P. Gobbi, and I. Koren (2006), Aerosol climatology using a tunable spectral variability cloud screening of AERONET data, *Geophys. Res. Lett.*, *33*, L07817, doi:10.1029/2005GL025478.

Koren, I., L. A. Remer, Y. J. Kaufman, Y. Rudich, and J. V. Martins (2007), On the twilight zone between clouds and aerosols, *Geophys. Res. Lett.*, *34*, L08805, doi:10.1029/2007GL029253.

Levelt, P. F., G. H. J. van den Oord, M. R. Dobber, A. Mälkki, H. Visser, J. de Vries, P. Stammes, J. Lundell, and H. Saari (2006), The Ozone Monitoring Instrument, *IEEE Trans. Geosci. Remote Sens.*, *44*(5), 1093–1101, doi:10.1109/TGRS.2006.872333.

Marshak, A., G. Wen, J. A. Coakley Jr., L. A. Remer, N. G. Loeb, and R. F. Cahalan (2008), A simple model for the cloud adjacency effect and the apparent bluing of aerosols near clouds, *J. Geophys. Res.*, *113*, D14S17, doi:10.1029/2007JD009196.

Martins, J. V., D. Tanré, L. Remer, Y. Kaufman, S. Mattoo, and R. Levy (2002), MODIS cloud screening for remote sensing of aerosols over oceans using spatial variability, *Geophys. Res. Lett.*, *29*(12), 8009, doi:10.1029/2001GL013252.

Meister, G., Y. Zhong, and C. R. McClain (2008), Derivation of the MODIS Aqua Point-Spread Function for ocean color bands, *Proc. SPIE Int. Soc. Opt. Eng.*, *7081*, 70811F, doi:10.1117/12.796980.

Nikolaeva, O. V., L. P. Bass, T. A. Germogenova, A. A. Kokhanovsky, V. S. Kuznetsov, and B. Mayer (2005), The influence of neighboring clouds on the clear sky reflectance with the 3-D transport code RADUGA, *J. Quant. Spectrosc. Radiat. Transfer*, *94*, 405–424, doi:10.1016/j.jqsrt.2004.09.037.

Perry, K. D., and P. V. Hobbs (1996), Influences of isolated cumulus clouds on the humidity of their surroundings, *J. Atmos. Sci.*, *53*, 159–174, doi:10.1175/1520-0469(1996)053<0159:IOICCO>2.0.CO;2.

Radke, L. F., and P. V. Hobbs (1991), Humidity and particle fields around some small cumulus clouds, *J. Atmos. Sci.*, *48*, 1190–1193, doi:10.1175/1520-0469(1991)048<1190:HAPFAS>2.0.CO;2.

Redemann, J., Q. Zhang, B. Schmid, P. B. Russell, J. M. Livingston, H. Jonsson, and L. A. Remer (2006), Assessment of MODIS-derived visible and near-IR aerosol optical properties and their spatial variability in the presence of mineral dust, *Geophys. Res. Lett.*, *33*, L18814, doi:10.1029/2006GL026626.

Remer, L. A., et al. (2005), The MODIS aerosol algorithm, products and validation, *J. Atmos. Sci.*, *62*, 947–973, doi:10.1175/JAS3385.1.

Rothman, L. S., and J. Schroeder (2002), Millennium HITRAN compilation, paper presented at 12th ARM Science Team Meeting, ARM Program, St. Petersburg, Fla., 8–12 April.

Rothman, L. S., K. Chance, J. Schroeder, and A. Goldman (2001), New edition of HITRAN database, paper presented at 11th ARM Science Team Meeting, ARM Program, Atlanta, Ga., 19–23 March.

Russell, P. B., et al. (1993), Pinatubo and Pre-Pinatubo Optical-Depth Spectra: Mauna Loa Measurements, Comparisons, Inferred Particle Size Distributions, Radiative Effects, and Relationship to Lidar Data, *J. Geophys. Res.*, *98*, 22,969–22,985.

Russell, P. B., J. M. Livingston, P. Hignett, S. Kinne, J. Wong, and P. V. Hobbs (1999), Aerosol-induced radiative flux changes off the United States mid-Atlantic coast, Comparison of values calculated from sunphotometer and in situ data with those measured by airborne pyranometer, *J. Geophys. Res.*, *104*, 2289–2307, doi:10.1029/1998JD200025.

Russell, P., et al. (2005), Aerosol optical depth measurements by airborne Sun photometer in SOLVE II: Comparisons to SAGE III, POAM III and airborne spectrometer measurements, *Atmos. Chem. Phys.*, *5*, 1311–1339.

Schmid, B., and C. Wehrli (1995), Comparison of Sun photometer calibration by Langley technique and standard lamp, *Appl. Opt.*, *34*, 4500–4512, doi:10.1364/AO.34.004500.

Schmid, B., et al. (2000), Clear sky closure studies of lower tropospheric aerosol and water vapor during ACE 2 using airborne Sun photometer, airborne in-situ, space-borne, and ground-based measurements, *Tellus, Ser. B*, *52*, 568–593, doi:10.1034/j.1600-0889.2000.00009.x.

Schmid, B., et al. (2001), Comparison of columnar water-vapor measurements from solar transmittance methods, *Appl. Opt.*, *40*, 1886–1896, doi:10.1364/AO.40.001886.

Spiegel, M. R., J. J. Schiller, and R. A. Srinivasan (2000), *Probability and Statistics*, 2nd ed., McGraw-Hill, New York.

Wen, G., A. Marshak, and R. F. Cahalan (2006), Impact of 3D clouds on clear sky reflectance and aerosol retrieval in a biomass burning region of Brazil, *IEEE Geosci. Remote Sens. Lett.*, *3*, 169–172, doi:10.1109/LGRS.2005.861386.

Yang, Y., and L. Di Girolamo (2008), Impacts of 3-D radiative effects on satellite cloud detection and their consequences on cloud fraction and aerosol optical depth retrievals, *J. Geophys. Res.*, *113*, D04213, doi:10.1029/2007JD009095.

Zhang, J., J. S. Reid, and B. N. Holben (2005), An analysis of potential cloud artifacts in MODIS over ocean aerosol optical thickness product, *Geophys. Res. Lett.*, *32*, L15803, doi:10.1029/2005GL023254.

J. M. Livingston, SRI International, 333 Ravenswood Avenue, Menlo Park, CA 94035, USA.

J. Redemann and Q. Zhang, BAER Institute, 560 Third Street W, Sonoma, CA 95476, USA. (jredemann@mail.arc.nasa.gov)

L. A. Remer, NASA Goddard Space Flight Center, Code 613.2, Greenbelt, MD 20771, USA.

P. B. Russell, NASA Ames Research Center, MS 245-5A, Moffett Field, CA 94035, USA.